Research Square

Preprints are preliminary reports that have not undergone peer review.
They should not be considered conclusive, used to inform clinical practice,
or referenced by the media as validated information.

Solar insolation and compound ENSO–Indian Ocean Dipole events jointly govern tree reproductive phenology across temporal scales in a dual-monsoon forest

T. Ganesh[1]

tganesh@atree.org

Ashoka Trust for Research in Ecology and the Environment

A. Saravanan[1]

Ashoka Trust for Research in Ecology and the Environment

S. Tamizhazhagan[1]

Ashoka Trust for Research in Ecology and the Environment

Deyatima Ghosh[2]

Indian Institute for Human Settlements

R. Ganesan[1]

Ashoka Trust for Research in Ecology and the Environment

M. Soubadra Devy[1]

Ashoka Trust for Research in Ecology and the Environment

Priya Davidar[3]

Research Article

Keywords: El Niño–Southern Oscillation, Indian Ocean Dipole, wavelet coherence, monsoon, Western Ghats

Posted Date: September 7th, 2026

DOI: https://doi.org/10.21203/rs.3.rs-10698581/v1

License: This work is licensed under a Creative Commons Attribution 4.0 International License. Read Full License

Additional Declarations: No competing interests reported.

Abstract

Tropical tree phenology integrates signals from local atmospheric conditions and ocean–atmosphere teleconnections, but their relative importance and the temporal scales at which they operate remain poorly resolved in monsoon-driven forests. We analysed 22 years (1991–2012) of monthly phenological observations from 864 trees of 71 species in a wet evergreen forest of the southern Western Ghats, India. Using generalised additive models (GAMs) to identify which climate variables predict each phenophase and at what lag, and wavelet coherence analysis to reveal at what temporal scale and when in the record each relationship was active, we quantified how community-level flowering and fruiting respond to local climate and to the El Niño–Southern Oscillation (ENSO) and Indian Ocean Dipole (IOD). Flowering was highly synchronous and concentrated in the first dry season, while fruiting was temporally dispersed. GAM and wavelet analysis showed flowering is related to insolation (lag 1 month), maximum temperature and minimum temperature (both lag 3 months), and fruiting is governed by minimum temperature at a six-month lag. Rainfall was not a significant predictor for either phenophases. Wavelet coherence confirmed ENSO as the more persistently coupled teleconnection overall, with IOD's influence restricted to dry seasons. Compound ENSO–IOD events produced the largest phenological anomalies in the record. These results demonstrate that flowering and fruiting are governed by distinct proximate climatic pathways, with teleconnections acting through different local variables at interannual scales, and that resolving these relationships requires both predictor-level significance testing and time-frequency analysis.

Introduction

The Asian monsoon, a seasonal reversal of winds and rainfall driven by land–sea thermal contrasts, structures the climate of much of South and Southeast Asia (Wang & Wu 2018). In peninsular India, two distinct rainfall regimes arise: the southwest monsoon (SWM; June–August), which covers most of the subcontinent, and the northeast monsoon (NEM; October–December), which brings rain to south-eastern India. The timing and intensity of both monsoon phases are modulated not only by regional solar forcing and atmospheric circulation but also by two basin-scale teleconnections: the El Niño–Southern Oscillation (ENSO) and the Indian Ocean Dipole (IOD) (Saji et al. 1999; Cai et al. 2014). ENSO affects South Asian climate primarily through monsoon circulation: El Niño events typically weaken SWM rainfall, elevate temperatures and alter cloud cover, whereas La Niña events tend to produce wetter conditions. The IOD, an independent but frequently co-occurring sea-surface-temperature gradient across the tropical Indian Ocean, can amplify or counteract ENSO depending on phase combination, generating substantial interannual variation in rainfall and temperature across peninsular India (Jiang et al. 2022). Because tropical tree reproduction responds strongly to variation in water availability, irradiance and temperature, both teleconnections have the potential to shape flowering and fruiting through local climatic pathways (Stuecker et al. 2017).

Tropical tree phenology is sensitive to climate variability because many species evolved under comparatively aseasonal conditions where small shifts in light, temperature or moisture act as strong reproductive cues (Zimmerman et al. 2007; Sakai 2001; Garwood et al. 2023). Flowering and fruiting are frequently synchronised to reductions in minimum temperature, increases in solar irradiance, or improved moisture availability (Mendoza et al. 2016; Wright & Calderón 2018; Chiang et al. 2021). Near the equator, where photoperiod varies minimally, irradiance alone predicts flowering (Garwood et al. 2023), whereas at higher tropical latitudes

flowering more often tracks changing day length (Borchert et al. 2015; Datta et al. 2025). Because reproductive development can span many months, phenological responses are sensitive not only to immediate climatic triggers but also to lagged effects of light, temperature and rainfall (Detto et al. 2018; Chen et al. 2017). Identifying which specific variables drive each phenophase, and at what lag, therefore requires both significance testing across multiple candidate predictors and tools that can detect when in a long record and at what periodicity each relationship is most active.

Multi-decadal phenology records remain rare outside a handful of long-studied tropical sites, leaving monsoon-influenced regions notably South Asia comparatively understudied (Mendoza et al. 2016; Sakai & Kitajima 2019). Where such records exist, ENSO effects on reproductive phenology prove highly variable: at Barro Colorado Island, Panama, flowering increased in El Niño years (Wright & Calderón 2006); in Southeast Asia, ENSO is responsible for Dipterocarp mast fruiting (Numata et al. 2003); in Uganda, fruit availability declines during ENSO-driven droughts (Chapman et al. 2018). ENSO's phenological footprint therefore varies markedly among continents, and the role of the IOD, despite its influence on the Asian monsoon, remains comparatively unexplored (Adamescu 2016). Compound ENSO–IOD events and their joint phenological consequences are particularly poorly understood in South Asian forests, even though the Western Ghats lie close to the centre of IOD-driven climate variability.

Within India, phenological monitoring has generally been short and concentrated in dry deciduous and evergreen forests of the south (Murali & Sukumar 1999; Ganesh & Davidar 2005; Ramaswami et al. 2019), with fewer studies from moist subtropical forests of the northeast (Shukla & Ramakrishnan 1982; Kikim & Yadava 2001). Two recent multi-year studies begin to close this gap: a long-term record from the Eastern Himalaya (Datta et al. 2025) and a phenology study from lowland dipterocarp forest elsewhere in the Western Ghats (Menon et al. 2025), both identifying climate variables as proximate drivers of reproductive timing. Both nonetheless underscore how few extended, systematic datasets exist for South Asia's forests, which support exceptional range-restricted biodiversity (Myers et al. 2000) and are experiencing intensifying climatic extremes.

Regions combining two monsoon seasons with exposure to multiple ocean–atmosphere teleconnections offer a natural test of how local and remote climate signals jointly structure phenology across temporal scales, yet such dual-monsoon systems have rarely been studied for more than a few years (Adamescu 2016; Chapman et al. 2018). The mid-elevation evergreen forests of the southern Western Ghats (900–1300 m) receive over 3500 mm of annual rainfall, roughly 50% from the NEM and 25–30% from the SWM (Ganesh et al. 1996), keeping the forest wet (> 100 mm month^{-1}) for about ten months of the year, with two distinct dry seasons: a pronounced one before the SWM (D1: January–May) and a shorter and wetter one before the NEM (D2: September). Frequent cloud cover and the bimodal rainfall regime suggest that solar insolation and temperature, rather than rainfall alone, may be the primary biometeorological cues governing reproductive timing. We therefore ask: (i) how seasonal is reproduction in this forest, and do the two phenophases operate on different temporal scales; (ii) which specific local climate variables, and at what lags, significantly predict flowering and fruiting; (iii) at what temporal scale and through which local climate pathways do ENSO and IOD modulate phenology; and (iv) do compound ENSO–IOD events amplify phenological responses beyond the effects of either teleconnection alone. Because ENSO's direct influence weakens outside the Pacific basin while the IOD is the primary basin-scale driver of Indian Ocean climate, we hypothesised that IOD would exert a stronger effect on phenology than ENSO.

Materials and methods

Study site

This study was conducted in a relatively undisturbed tropical mid-elevation wet evergreen forest at Kakachi (8°33'N, 77°23'E), within the Kalakad-Mundanthurai Tiger Reserve, southern Western Ghats, India (Fig. S1). Kakachi lies at 1300 m elevation and receives over 3500 mm of rainfall annually, distributed across the SWM (June–August) and NEM (October–December), with two dry seasons: D1 (January–May) and D2 (September) (Ganesh et al. 1996; Fig. 1). The vegetation is a mid-elevation wet evergreen forest characterised by high endemism, dominated by Cullenia exarillata, Palaquium ellipticum and Aglaia bourdillonii (Ganesh et al. 1996; Pascal et al. 2004). Pollination and dispersal systems of the tree community have been described previously (Devy 2001; Devy & Davidar 2003; Ganesh & Davidar 2001), and the site's soils are nutrient-poor and acidic (Vishnu et al. 2023).

Phenological data collection

Phenological monitoring of canopy and sub-canopy trees began in January 1991. At Kakachi, 729 individuals from 87 species (>10 cm DBH) were tagged with numbered aluminium plates and observed monthly along trails covering ~25 km² of undisturbed forest; an additional ~6 km² was monitored at the selectively logged Upper Kodayar forest (Table S1). We retained only species represented by five or more individuals, yielding a final dataset of 71 species and 864 individuals. Each month, observers visually estimated the proportion of each crown covered by six phenophases to the nearest 10%: leaf flush, dry leaves, flower buds, open flowers, unripe fruit and ripe fruit, following the canopy-cover scoring protocol of Chapman et al. (2018). A phenophase was scored as present if it covered ≥1% of the visible crown; community-level flowering and fruiting proportions are the cross-species mean of individual scores. Analyses focus on the flowering and fruiting phenophases over the 22-year record (1991–2012). More details are in the supplementary materials.

Environmental data

Local daily rainfall and maximum and minimum temperature were obtained from the Manimuthar tea estate meteorological station, 5 km from the study site at equivalent elevation and habitat. Monthly incoming solar insolation (kWh m^{-2} day^{-1}) was obtained from the NASA POWER database (https://power.larc.nasa.gov/; NASA 2020). The Oceanic Niño Index (ONI), used to characterise ENSO phase, and the Dipole Mode Index (DMI), used to characterise IOD phase, were obtained from the NOAA Physical Sciences Laboratory (https://psl.noaa.gov). El Niño and La Niña months were defined as ONI > 0.5 °C or < −0.5 °C sustained for at least five consecutive months; positive and negative IOD months were defined as DMI > 0.5 °C or < −0.5 °C sustained for at least three consecutive months. Full station and database details are provided in the Supplementary Material.

Data analysis

We used two analytical frameworks that address distinct and complementary aspects of the climate–phenology relationship. GAMs identify which climate variables are significant predictors of each phenophase,

the specific lag at which each operates, and how much variance each explains requires a regression framework with significance testing across candidate predictors. Wavelet coherence analysis reveals at what temporal scale and when in the 22-year record each climate–phenophase relationship was active, questions that require a time-frequency framework capable of detecting non-stationary associations. Together they characterise both the identity of the proximate drivers and the temporal structure of their effects.

Generalised additive models. GAMs with beta regression were fitted separately for community-level flowering and fruiting proportions. Photoperiod was excluded as a candidate predictor: at the study latitude of 8.3°N, annual daylength variation is only ~1 hour, causing photoperiod to co-vary almost perfectly with the seasonal insolation and temperature cycle; it cannot be distinguished statistically as an independent physiological driver and its inclusion would conflate a calendar-date proxy with the mechanistic climatic predictors of interest (Wright & van Schaik 1994; Borchert et al. 2015; Garwood et al. 2023). Candidate predictors were insolation, maximum temperature, minimum temperature, rainfall, ONI and DMI, each tested as smooth terms at monthly lags from 0 to 12 months; the lag maximising explained deviance was retained per predictor. This window spans the full range of plausible mechanisms, from immediate physiological triggers (lags 0–2 months) to fruit-maturation lags of up to one year (Detto et al. 2018; Zimmerman et al. 2007). We compared nested models using AIC and deviance explained (Table S2): a seasonal-climate-only baseline (Snp: all local predictors at optimal lags, plus cyclic month and year smooths), models adding ONI or DMI individually, and a full model adding both teleconnections. Model selection followed the principle of minimum AIC; all models include cyclic-month and year-trend smooths to account for residual seasonality and long-term change. Predictor-level effects (χ^2, p, effective degrees of freedom) for the best-supported model of each phenophase are reported in Table 1. Long-term trends were assessed with Mann–Kendall tests.

Wavelet coherence. Wavelet coherence was computed between each phenophase and each local climate variable and teleconnection index. Significant coherence regions ($p < 0.05$) were identified against red-noise surrogates, and phase relationships (leads and lags) were read from the phase-angle information within significant regions. Mean squared wavelet coherence averaged across the full time-frequency plane was computed for every climate–phenophase pair to provide a ranked summary of overall coupling strength (Table 1). Monthly time series were also band-pass filtered to isolate interannual variability (approximately 1.5–8-year periods) for assessing temporal concordance during compound ENSO–IOD events. Kruskal–Wallis H tests were used to compare local climate variables among ENSO and IOD phases within each season. All wavelet analyses were performed using the biwavelet package (v0.14) in R 4.5.1. Full specifications are given in the Supplementary Material.

Results

Seasonal phenology and interannual variation

On average, 61% of species flowered during March–April (D1), with less than 1% of individuals flowering outside their primary dry-season window (Fig. 2). Lower-intensity flowering occurred during the SWM and NEM, and approximately 4% of species flowered twice annually. Fruiting was more evenly distributed across the year, with peaks in May–June and August–September, and approximately 11% of species fruited continuously or bimodally. Circular statistics confirmed strong flowering seasonality (mean vector strength $r = 0.71$, $p < 0.001$,

clustering around a mid-April mean date), whereas fruiting was more dispersed around an early-June mean ($r = 0.42$, $p < 0.001$), with a secondary October peak (Fig. 2). Wavelet power spectra revealed dominant periodicities of 6–7 months for flowering and 12 months for fruiting (Fig. S2), confirming that the two phenophases operate on fundamentally distinct temporal scales.

Community-level flowering and fruiting showed strong interannual variation over the 22 years (Fig. 3), with coefficients of variation of 57% and 45% respectively, compared with 10–13% for local climate variables. Mann–Kendall tests revealed a significant long-term decrease in the proportion of trees flowering ($Z = -0.16$, $p = 0.001$) but no significant trend in fruiting ($Z = 0.078$, $p = 0.059$). Minimum temperature decreased significantly ($Z = -4.06$, $p < 0.001$) and maximum temperature increased ($Z = 3.08$, $p = 0.002$), while rainfall and solar radiation showed no significant directional trends.

Proximate climatic drivers

GAMs identified distinct predictor sets for the two phenophases, with the best-supported flowering model being S + IOD ($\Delta AIC = -8.8$ relative to the seasonal-climate baseline S, deviance explained 48.9%, Adj. $R^2 = 0.462$) and the best-supported fruiting model being S + ENSO + IOD ($\Delta AIC = -52.3$, deviance 58.7%, Adj. $R^2 = 0.501$; full model comparison in Table S2). Predictor-level effects for the two best-supported models are given in Table 1.

Flowering was significantly predicted by insolation at a one-month lag ($\chi^2 = 5.43$, $p = 0.020$), maximum temperature at a three-month lag ($\chi^2 = 9.2$, $p = 0.016$) and minimum temperature at the same lag ($\chi^2 = 4.63$, $p = 0.032$), together defining a warm, bright, pre-monsoon signal as the proximate flowering cue. IOD was the only teleconnection significantly retained in the flowering model (lag 6, edf = 2.47, $\chi^2 = 11.0$, $p = 0.013$; $\Delta AIC = -8.8$); ENSO added only marginal improvement ($\Delta AIC = -0.3$) and was not significant at any lag ($p > 0.15$). Rainfall was not significant for flowering in any model.

Fruiting was governed principally by minimum temperature at a six-month lag (edf = 3.01, $\chi^2 = 18.9$, $p < 0.001$, strongly nonlinear). Both ENSO (lag 9, edf = 2.07, $\chi^2 = 12.5$, $p = 0.004$) and IOD (lag 11, edf = 4.09, $\chi^2 = 15.8$, $p = 0.005$) were significantly retained for fruiting. SNP+ENSO alone improved fruiting fit substantially ($\Delta AIC = -39.9$, deviance 54.6%), SNP + IOD alone was similar ($\Delta AIC = -40.6$, deviance 55.5%), and a teleconnection-only model (ENSO + IOD, no local climate terms) explained 54.9% of fruiting deviance ($\Delta AIC = -47.0$), confirming both teleconnections as dominant interannual drivers of fruiting intensity independently of local climate. Rainfall was not significant for fruiting in any model. The highly significant year-trend smooth retained in both models (flowering: $\chi^2 = 34.3$, $p < 0.001$; fruiting: $p < 0.001$) indicates pronounced long-term change in both phenophases not fully accounted for by the seasonal predictors or teleconnection indices included.

Temporal scale and persistence of climate–phenology relationships

Wavelet coherence revealed the temporal structure behind the GAM results, showing when in the 22-year record each relationship was active and at what periodicity (Fig. 4; Table 1). Among local climate variables, insolation showed the highest mean squared coherence with flowering ($R^2 = 0.551$) and fruiting ($R^2 = 0.492$), with coherence concentrated at seasonal-to-annual periodicities and insolation leading flowering by

approximately one to two months within significant regions consistent with the one-month lag identified by the GAM. Maximum temperature showed strong coherence with flowering (R^2 = 0.471), co-varying with insolation at the same pre-monsoon window. Minimum temperature was most strongly associated with fruiting (R^2 = 0.439), with fruiting lagging minimum temperature by approximately five to six months within significant wavelet regions, consistent with the six-month lag in the GAM. Rainfall showed weaker and more intermittent coherence with both phenophases (flowering R^2 = 0.390; fruiting R^2 = 0.433), consistent with its non-significance as a concurrent predictor in the GAMs.

Wavelet coherence between the teleconnection indices and phenology was weaker than that between local climate and phenology (Fig. 5). ENSO showed stronger overall coupling than IOD for both phenophases (fruiting: 0.393 vs. 0.374; flowering: 0.362 vs. 0.355) and for every local climate variable (Table 1), confirming ENSO as the more broadly and persistently coupled teleconnection across the full record. This contrasts with the GAM result, where IOD, not ENSO was the only significant teleconnection predictor of flowering. The two results are not contradictory: the GAM captures a seasonally concentrated IOD signal that recurs reliably at a fixed six-month lag within the critical flowering window, whereas the whole-record wavelet average is insensitive to such temporal concentration, and instead reflects ENSO's broader and more sustained coupling with local climate across all seasons. IOD's coherence with local climate was largely confined to 2005–2012 and concentrated on minimum temperature; ENSO's coupling with minimum temperature was the strongest and most persistent of all teleconnection–local-climate pairs (peak $R^2 > 0.75$, 2–4-year band, 1994–2012), with El Niño years coinciding with elevated minimum temperatures, and a persistent anti-phase ENSO–rainfall relationship in the same band.

Compound ENSO–IOD events

Band-pass filtering revealed strong interannual synchrony between flowering and fruiting anomalies during prolonged La Niña events, suggesting both phenophases share a common interannual forcing during certain periods (Fig. 6). The strongest phenological anomalies in the 22-year record clustered around ENSO–IOD co-occurrences. During 1997–1998, a strong El Niño and positive IOD coincided, simultaneously suppressing insolation and elevating temperatures and producing climate anomalies larger than either mode alone. Flowering rose above the long-term baseline during this compound period, while fruiting was initially suppressed before rebounding strongly once La Niña–negative-IOD conditions restored rainfall and insolation. Because the largest departures in both phenophases cluster around these rare compound windows, interannual reproductive variability in this system appears to be disproportionately driven by compound teleconnection states rather than the steady additive influence of either mode operating independently.

Discussion

Seasonal phenology: a dry-season pulse and a year-round continuum

Flowering in Kakachi was highly synchronised within the community, overwhelmingly concentrated in D1, with wavelet power spectra confirming a sub-annual rhythm to this synchrony. This concentration is consistent with selection for mast-like reproductive timing under pollinator-availability and predator-satiation pressures

(Augspurger 1982; Ashton et al. 1988; Sakai 2001), and mirrors dry-season flowering peaks documented at other Western Ghats sites and in the Eastern Himalaya (Krishnan 2002; Nanda et al. 2014; Datta et al. 2025; Menon et al. 2025). Fruiting was far more dispersed across the year and constrained to an annual rather than sub-annual periodicity — a temporal decoupling widely reported from Neotropical and other Asian forests (van Schaik 1986; Zimmerman et al. 2007; Chang-Yang et al. 2016; Mendoza et al. 2016).

This decoupling reflects the developmental cost of fruit maturation. Converting a flower into a mature fruit requires sustained carbon and water allocation over several months, and species initiating fruit development in the cooler post-monsoon period likely draw on carbohydrate reserves accumulated during the preceding high-irradiance dry season (Rathcke & Lacey 1985; Bawa et al. 2003; Garwood et al. 2023). The extended, staggered fruit retention at Kakachi is evident in dominant species such as *Cullenia exarillata* and *Myristica beddomei*, which hold immature fruit for the better part of a year; hard or spiny endocarps in several dominant species likely represent an evolved defence against prolonged predation traded off against slower development (Ganesh 1996; Ganesh & Davidar 2001, 2005). Flowering is therefore a fast, highly synchronised, seasonally triggered event, while fruiting is a slow, resource-limited, and individually staggered process constrained to complete within an annual cycle regardless of when flowering occurred.

Distinct proximate pathways for flowering and fruiting

Both the GAM and wavelet coherence results converge on the same proximate drivers for flowering: a warm, bright pre-monsoon signal characterised by rising insolation and maximum temperature in the weeks to months before anthesis. The GAM identified insolation at a one-month lag, maximum temperature at three months and minimum temperature at three months as jointly significant, and wavelet coherence independently placed insolation as the highest-ranking driver across the full 22-year record, leading flowering by approximately one to two months within significant regions. The close correspondence between the one-month GAM lag and the wavelet phase displacement is reassuring: the same signal emerges whether we ask which predictor best explains phenological variance at a fixed lag or which variable co-varies most persistently with phenology across time and scale. This is consistent with photoinductive-threshold models in which rising irradiance above a critical level promotes floral initiation (Wright & van Schaik 1994; Zimmerman et al. 2007; Wright & Calderón 2018; Borchert et al. 2015; Menon et al. 2025). The three-month maximum and minimum temperature lags reflect the thermal pre-conditioning required before anthesis a pattern also documented in the Eastern Himalaya, where temperature over several pre-flowering months was the strongest predictor of flowering timing (Datta et al. 2025).

Fruiting responded to an entirely different, longer-lagged signal: minimum temperature at a six-month lag was the dominant GAM predictor with a strongly nonlinear form, and wavelet coherence showed fruiting lagging minimum temperature by approximately five to six months within significant regions. The close agreement between the GAM lag and the wavelet phase displacement again provides mutual reinforcement between the two analytical frameworks. The six-month lag corresponds closely to the angular separation between the circular mean dates of flowering and fruiting, consistent with a developmental model in which fruit maturation follows a timeline set largely at the time of flowering itself. The non-significance of rainfall as a concurrent predictor for either phenophase in all GAM models, combined with its weaker and more intermittent wavelet coherence relative to temperature and insolation, reflects the moisture buffering of Kakachi's dual-monsoon regime, where wet conditions persist for approximately ten months of the year. This contrasts with rainfall-

driven phenological systems documented in drier tropical regions (Dunham et al. 2011, 2018; Mendoza et al. 2016) and attributes the relative unimportance of local rainfall variability to the sustained high moisture baseline of this dual-monsoon system rather than to an absence of a rainfall response per se.

Teleconnections: distinct pathways, complementary evidence

The GAM and wavelet results offer complementary perspectives on how ENSO and IOD reach phenology, and their apparent disagreement over the relative importance of the two modes for flowering is informative rather than contradictory. The GAM retained IOD and not ENSO as the only significant teleconnection predictor of flowering, while wavelet coherence ranked ENSO as the more persistently and broadly coupled teleconnection for every local climate variable for both phenophases at the whole-record scale. This reflects where each mode's influence is concentrated. IOD events in this record were typically brief (fewer than three consecutive months in most years) and concentrated in the D1 and NEM periods, where negative-IOD conditions locally elevated insolation and minimum temperature, precisely the pre-monsoon warm-and-bright signal to which flowering is tuned. A fixed six-month-lag GAM regression detects this signal because it recurs reliably in a specific seasonal window while a whole-record wavelet average does not. ENSO's coupling with local climate, by contrast, was broad, with a persistent in-phase control of minimum temperature at 2–4-year intervals, combined with an anti-phase rainfall relationship in the same band (Jayanthi & Govindachari 1999; Sengupta & Sumant 2019). Because minimum temperature is also the dominant local driver of fruiting at a six-month lag, ENSO's interannual thermal signal is transmitted preferentially into fruiting rather than flowering, a pattern consistent with ENSO's global prominence as a driver of tropical fruit production (Wright et al. 1999; Wright & Calderón 2006; Chapman et al. 2005, 2018; Numata et al. 2003). IOD contributed independently to fruiting at an eleven-month lag in the GAM, indicating that fruit production integrates teleconnection-mediated climate signals accumulated over the better part of a year, consistent with its status as a slow, resource-limited process.

The dual-monsoon regime shapes the relative roles of the two teleconnections by buffering the sharp moisture deficits that drive ENSO-coupled mast reproduction in single-monsoon systems such as Borneo (Ashton et al. 1988; Sakai 2001). This limits ENSO's capacity to produce the brief, sharply timed moisture stress to which flowering appears tuned, while leaving its slower, cumulative thermal pathway into fruiting intact. Our initial hypothesis that IOD would exert a stronger overall influence than ENSO was only partially supported: IOD is the more relevant modulator of flowering within the specific seasonal window that matters for anthesis, while ENSO is the more persistently and broadly coupled driver of interannual climate variability and of fruiting.

Compound events and broader implications

The largest phenological anomalies in the 22-year record clustered around compound ENSO–IOD co-occurrences rather than episodes of either mode alone, and both phenophases tracked this amplification. Compound events, most strikingly in 1997–1998, produced climate anomalies that exceeded what either teleconnection generates independently, suggesting that models treating ENSO and IOD as additive independent predictors may systematically underestimate their combined ecological impact (Stuecker et al. 2017). Given that El Niño and positive-IOD events are both projected to become more frequent under continued greenhouse warming (Cai et al. 2014; Jiang et al. 2022), compound windows may become increasingly important drivers of interannual reproductive variability in dual-monsoon forests, with cascading effects on

frugivore populations and seedling recruitment (Chapman et al. 2005; Butt et al. 2015). Future analysis will need to keep these in mind to interpret phenology response to changing climate

The significant long-term decline in flowering, concurrent with increasing maximum temperature and decreasing minimum temperature, is consistent with growing evidence that tropical phenology is shifting in response to climate change (Corlett & Lafrankie 1998; Butt et al. 2015; Sheldon 2019). The highly significant year-trend smooth retained in both GAMs, independent of the seasonal and teleconnection predictors, points to a further decadal-scale driver possibly mediated by the nutrient-poor, acidic soils of the southern Western Ghats (Vishnu et al. 2023; Tanner et al. 1998; Dalling et al. 2016) that warrants continued monitoring as the record lengthens. The climatic controls of flowering and fruiting also cascade into forest demography: the timing of fruit ripening relative to the onset of the SWM sets the moisture window for immediate germination of recalcitrant seeds in several dominant species such as *Palaquium ellipticum, Myristica beddomei* and many *Litsea* species, linking interannual teleconnection variability to seedling recruitment and longer-term compositional change (Foster 1982; Chapman et al. 2018; Lebrija-Trejos et al. 2023).

Several limitations constrain the generality of our findings. Insolation data were satellite-derived at coarse spatial resolution and may not capture within-canopy light variation in this structurally complex forest (Tang & Dubayah 2017; Oliveira & Zhang 2025). We treated the community as a single pooled unit, whereas canopy, understorey and edge species likely respond differently to the same regional climate signal (Boyle & Bronstein 2012; Vinod et al. 2023; Nunes et al. 2022). The predictor set omitted vapour pressure deficit, soil moisture and cloud cover, each of which can independently shape canopy phenology (Detto et al. 2018; Vinod et al. 2023). Finally, this study addressed only flowering and fruiting; extending the approach to leaf flushing and senescence would provide a more integrated view of climate controls on phenology across the annual cycle (Newstrom et al. 1994).

Conclusion

This 22-year analysis shows that community-level flowering and fruiting in a dual-monsoon wet evergreen forest of the southern Western Ghats are governed by distinct proximate climatic pathways. Flowering is a fast, synchronised, sub-annual pulse best predicted by insolation at a one-month lag and by maximum and minimum temperature at three-month lags, with IOD amplifying the pre-monsoon thermal and radiative signal episodically. Fruiting is a slow, annually constrained, resource-limited process governed by minimum temperature at a six-month lag and modulated interannually by both ENSO and IOD. Compound ENSO–IOD events produce phenological anomalies that exceed those of either mode alone, and the largest departures in the record cluster around these rare compound states. The apparent difference between GAM and wavelet results on the relative importance of ENSO and IOD for flowering is not a discrepancy but a complementary view: GAMs identify what recurs reliably at a specific seasonal lag, while wavelet coherence captures what is most broadly and persistently coupled across the full record. Both frameworks together are needed, and both confirm that ENSO and IOD must be modelled jointly, including their compound phases when projecting phenological responses to future climate change in monsoon-influenced tropical forests.

Declarations

Funding: This work was supported by the Ministry of Environment, Forests and Climate Change (Government of India), the MacArthur Foundation (through Prof. Kamal Bawa), the Department of Science and Technology (Government of India), the Royal Norwegian Embassy, the Rufford Foundation, the International Foundation for Science, the Tata Trust, and CSR contributions from Brakes India and Sundaram Finance.

Conflicts of interest: The authors declare no competing interests.

Ethics approval: Field monitoring was conducted under permission from the Tamil Nadu Forest Department; no experimental manipulation of protected species was involved.

Data availability: Phenology and local climate datasets are available from the corresponding author on reasonable request.

Author contributions: [To be supplied — please use the CRediT taxonomy as required by Springer/IJB guidelines.]

Acknowledgements

We thank the Tamil Nadu Forest Department for permission to conduct long-term research in the Kalakad-Mundanthurai Tiger Reserve, the Tamil Nadu Electricity Board for logistic support, and Bombay Burma Trading Company for weather data. We thank Prof. Kamal Bawa for continued support and comments on the manuscript, Prof. Joseph Wright for invaluable advice, Asmita Sengupta and K. S. Seshadri for helpful suggestions, and Rani Krishnan for assistance with tree identification.

References

1. Adamescu GS (2016) Impacts of global climate change on the phenology of African tropical ecosystems. MSc thesis, University of York, UK
2. Ashton PS, Givnish TJ, Appanah S (1988) Staggered flowering in the Dipterocarpaceae: new insights into floral induction and the evolution of mast fruiting in the aseasonal tropics. Am Nat 132:44–66
3. Augspurger CK (1982) A cue for synchronous flowering. In: Leigh EG, Rand AS, Windsor DM (eds) The ecology of a neotropical forest: seasonal rhythms and long-term changes. Smithsonian Institution, Washington DC, pp 133–150
4. Bawa KS, Kang H, Grayum MH (2003) Relationships among time, frequency, and duration of flowering in tropical rain forest trees. Am J Bot 90:877–887
5. Borchert R, Calle Z, Strahler AH, Baertschi A, Magill RE, Broadhead JS, Lopez D (2015) Insolation and photoperiodic control of tree development near the equator. New Phytol 205:7–13
6. Boyle WA, Bronstein JL (2012) Phenology of tropical understory trees: patterns and correlates. Rev Biol Trop 60:1415–1430
7. Butt N, Seabrook L, Maron M, Law BS, Dawson TP, Syktus J (2015) Cascading effects of climate extremes on vertebrate fauna through changes to low-latitude tree flowering and fruiting phenology. Glob Chang Biol 21:3267–3277
8. Cai W, Borlace S, Lengaigne M et al (2014) Increasing frequency of extreme El Niño events due to greenhouse warming. Nat Clim Chang 4:111–116. https://doi.org/10.1038/nclimate2100

9. Chang-Yang CH, Sun IF, Tsai CH, Lu CL, Hsieh CF (2016) ENSO and frost codetermine decade-long temporal variation in flower and seed production in a subtropical rain forest. J Ecol 104:44–54
10. Chapman CA, Chapman LJ, Zanne AE, Poulsen JR, Clark CJ (2005) A 12-year phenological record of fruiting: implications for frugivore populations and indicators of climate change. In: Dew JL, Boubli JP (eds) Tropical fruits and frugivores. Springer, Netherlands, pp 75–92
11. Chapman CA, Valenta K, Bonnell TR, Brown KA, Chapman LJ (2018) Solar radiation and ENSO predict fruiting phenology patterns in a 16-year record from Kibale National Park. Uganda Biotropica 50:384–395
12. Chen X, Wang L, Inouye D (2017) Delayed response of spring phenology to global warming in subtropics and tropics. Agric Meteorol 234:222–235
13. Chiang JCH, Friedman AR, Vimont DJ (2021) ENSO and climate variability. Annu Rev Earth Planet Sci 49:1–30
14. Corlett RT, Lafrankie JV (1998) Potential impacts of climate change on tropical Asian forests through an influence on phenology. Clim Chang 39:439–453
15. Dalling JW, Heineman K, Lopez OR, Wright SJ, Turner BL (2016) Nutrient availability in tropical rain forests: the paradigm of phosphorus limitation. In: Goldstein G, Santiago L (eds) Tropical tree physiology. Springer, Cham, pp 261–274
16. Datta A, Banerjee S, Naniwadekar R, Thapa K, Rathore A, Thapa K, Brah T, Nabum T, Mogar N, Shukla U, Sidhu S, Borawake N (2025) Patterns of leaf, flower, and fruit phenology and environmental relationships in a seasonal tropical forest in the Indian Eastern Himalaya. Biotropica 57:e70030. https://doi.org/10.1111/btp.70030
17. Detto M, Wright SJ, Calderón O et al (2018) Resource acquisition and reproductive strategies of tropical forest in response to the El Niño–Southern Oscillation. Nat Commun 9:913. https://doi.org/10.1038/s41467-018-03306-9
18. Devy MS (2001) Pollination ecology of wet evergreen forest trees in the Western Ghats. J Biosci 26:427–437
19. Devy MS, Davidar P (2003) Pollination systems of trees in Kakachi, a mid-elevation wet evergreen forest in the Western Ghats, India. Am J Bot 90:650–657
20. Dunham AE, Erhart EM, Wright PC (2011) Global climate cycles and cyclones: consequences for rainfall patterns and lemur reproduction in southeastern Madagascar. Glob Chang Biol 17:219–227
21. Dunham AE, Razafindratsima OH, Rakotonirina P, Wright PC (2018) Fruiting phenology is linked to rainfall variability in a tropical rain forest. Biotropica 50:396–404
22. Foster RB (1982) The seasonal rhythm of fruitfall on Barro Colorado Island. In: Leigh EG, Rand AS, Windsor DM (eds) The ecology of a neotropical forest. Smithsonian Institution, Washington DC, pp 151–172
23. Ganesh T (1996) Fruiting patterns among canopy trees and fruit use by vertebrates in a wet evergreen forest of southern Western Ghats, India. PhD dissertation, Pondicherry University, Puducherry, India
24. Ganesh T, Ganesan R, Devy MS, Davidar P, Bawa KS (1996) Assessment of plant biodiversity at a mid-elevation evergreen forest of Kalakad Mundanthurai Tiger Reserve, Western Ghats, India. Curr Sci 71:379–392
25. Ganesh T, Davidar P (2001) Dispersal modes of tree species in the wet evergreen forests of the Western Ghats. Curr Sci 80:394–399

26. Ganesh T, Davidar P (2005) Fruiting phenology and pre-dispersal seed predation in a rainforest in southern Western Ghats, India. In: Dew JL, Boubli JP (eds) Tropical fruits and frugivores. Springer, Netherlands, pp 137–152
27. Garwood NC, Metz MR, Queenborough SA, Persson V, Wright SJ, Burslem DF, Valencia R (2023) Seasonality of reproduction in an ever-wet lowland tropical forest in Amazonian Ecuador. Ecology 104:e4133
28. Jayanthi N, Govindachari S (1999) El Niño and NE monsoon rainfall over Tamil Nadu. Mausam 50:217–218
29. Jiang J, Liu Y, Mao J, Li J, Zhao S, Yu Y (2022) Three types of positive Indian Ocean Dipoles and their relationships with the South Asian summer monsoon. J Clim 35:405–424
30. Kikim A, Yadava PS (2001) Phenology of tree species in subtropical forests of Manipur, north eastern India. Trop Ecol 42:269–276
31. Krishnan RM (2002) Reproductive phenology of a wet forest understorey in the Western Ghats, south India. Glob Ecol Biogeogr 11:179–182
32. Lebrija-Trejos E, Hernández A, Wright SJ (2023) Effects of moisture and density-dependent interactions on tropical tree diversity. Nature 615:100–104
33. Mendoza I, Peres CA, Morellato LPC (2016) Continental-scale patterns and climatic drivers of fruiting phenology: a quantitative Neotropical review. Glob Planet Change. https://doi.org/10.1016/j.gloplacha.2016.12.001
34. Menon D, Behera D, Ayyappan N (2025) Phenological trends and associated climate drivers of a tree community in lowland dipterocarp forest, Western Ghats, India. Int J Biometeorol 69:177–193. https://doi.org/10.1007/s00484-024-02802-6
35. Murali KS, Sukumar R (1999) Leaf flushing phenology and herbivory in a tropical dry deciduous forest, southern India. Oecologia 94:114–119
36. Murtugudde R, Busalacchi AJ (1999) Interannual variability of the dynamics and thermodynamics of the tropical Indian Ocean. J Clim 12:2300–2326
37. Myers N, Mittermeier RA, Mittermeier CG et al (2000) Biodiversity hotspots for conservation priorities. Nature 403:853–858
38. Nanda A, Suresh HS, Krishnamurthy YL (2014) Phenology of a tropical dry deciduous forest of Bhadra Wildlife Sanctuary, southern India. Ecol Process 3:1. https://doi.org/10.1186/2192-1709-3-1
39. NASA (2020) NASA POWER: solar data overview. https://power.larc.nasa.gov/docs/methodology/solar/
40. Newstrom LE, Frankie GW, Baker HG (1994) A new classification for plant phenology based on flowering patterns in lowland tropical rain forest trees at La Selva, Costa Rica. Biotropica 26:141–159
41. Nunes MH, Camargo JLC, Vincent G, Calders K, Oliveira RS, Huete A, Mendes de Moura Y, Nelson B, Smith MN, Stark SC, Maeda EE (2022) Forest fragmentation impacts the seasonality of Amazonian evergreen canopies. Nat Commun 13:917
42. Numata S, Yasuda M, Okuda T, Kachi N, Noor NSM (2003) Temporal and spatial patterns of mass flowerings on the Malay Peninsula. Am J Bot 90:1025–1031
43. Oliveira PV, Zhang X (2025) Upper canopy and understory phenology of Brazilian Amazon forests seen by GEDI lasers. Environ Res Lett 20:044015

44. Pascal JP, Ramesh BR, Franceschi D (2004) Wet evergreen forest types of the southern Western Ghats, India. Trop Ecol 45:281–292
45. Ramaswami G, Datta A, Reddy A, Quader S (2019) Tracking phenology in the tropics and in India: the impacts of climate change. In: The implications of climate change for Indian biodiversity: an overview, pp 45–59
46. Rathcke B, Lacey EP (1985) Phenological patterns of terrestrial plants. Annu Rev Ecol Syst 16:179–214
47. Saji NH, Goswami BN, Vinayachandran PN, Yamagata T (1999) A dipole mode in the tropical Indian Ocean. Nature 401:360–363
48. Sakai S (2001) Phenological diversity in tropical forests. Popul Ecol 43:77–86
49. Sakai S, Kitajima K (2019) Tropical phenology: recent advances and perspectives. Ecol Res 34:50–54
50. Schott FA, Xie S-P, McCreary JP Jr (2009) Indian Ocean circulation and climate variability. Rev Geophys 47:RG1002. https://doi.org/10.1029/2007RG000245
51. Sengupta A, Sumant N (2019) The northeast winter monsoon over the Indian subcontinent and southeast Asia. J Clim 32:231–249
52. Sheldon KS (2019) Climate change in the tropics: ecological and evolutionary responses at low latitudes. Annu Rev Ecol Evol Syst 50:303–333
53. Shukla RP, Ramakrishnan PS (1982) Phenology of trees in a sub-tropical humid forest in north-eastern India. Vegetatio 49:103–109
54. Stenseth NC, Mysterud A (2005) Weather packages: finding the right scale and composition of climate in ecology. J Anim Ecol 74:1195–1198
55. Stuecker MF, Timmermann A, Jin FF, Chikamoto Y, Zhang W, Wittenberg AT, Widiasih E, Zhao S (2017) Revisiting ENSO/Indian Ocean Dipole phase relationships. Geophys Res Lett 44:2481–2492. https://doi.org/10.1002/2016GL072308
56. Tang H, Dubayah R (2017) Light-driven growth in Amazon evergreen forests explained by seasonal variations of vertical canopy structure. Proc Natl Acad Sci USA 114:2640–2644
57. Tanner EVJ, Vitousek PM, Cuevas E (1998) Experimental investigation of nutrient limitation of forest growth on wet tropical mountains. Ecology 79:10–22
58. Van Schaik CP (1986) Phenological changes in a Sumatran rain forest. J Trop Ecol 2:327–347
59. Vinod N, Slot M, McGregor IR, Ordway EM, Smith MN, Taylor TC, Sack L, Buckley TN, Anderson-Teixeira KJ (2023) Thermal sensitivity across forest vertical profiles: patterns, mechanisms, and ecological implications. New Phytol 237:22–47
60. Vishnu PS, Sandeep S, Anil Kumar KS (2023) Taxonomy and genesis of soils in contrasting ecosystems of southern Western Ghats, India. CATENA 231:107325
61. Wang C, Wu L (2018) Future changes of the monsoon trough: sensitivity to sea surface temperature gradient and implications for tropical cyclone activity. Earth's Future 6:919–936. https://doi.org/10.1029/2018EF000858
62. Wright SJ, van Schaik CP (1994) Light and the phenology of tropical trees. Am Nat 143:192–199
63. Wright SJ, Carrasco C, Calderón O, Paton S (1999) The El Niño Southern Oscillation, variable fruit production, and famine in a tropical forest. Ecology 80:1632–1647

64. Wright SJ, Calderón O (2006) Seasonal, El Niño and longer-term changes in flower and seed production in a moist tropical forest. Ecol Lett 9:35–44
65. Wright SJ, Calderón O (2018) Solar irradiance as the proximate cue for flowering in a tropical moist forest. Biotropica 50:374–383
66. Zimmerman JK, Wright SJ, Calderón O, Pagán MA, Paton S (2007) Flowering and fruiting phenologies of seasonal and aseasonal Neotropical forests: the role of annual changes in irradiance. J Trop Ecol 23:231–251

Tables

Table 1. Combined GAM and wavelet coherence results for each predictor–phenophase combination. GAM columns (Lag, edf, χ^2, p): predictor-level effects in the best-supported model for each phenophase (flowering: S + IOD, deviance explained 48.9%, Adj. R^2 = 0.462, ΔAIC = −8.8 relative to **S** baseline; fruiting: Snp + ENSO + IOD, deviance 58.7%, Adj. R^2 = 0.501, ΔAIC = −52.3). Wavelet coherence column (Wav R^2): mean squared wavelet coherence averaged across the full time–frequency plane, providing a summary of overall coupling strength across the 22-year record regardless of GAM significance. **S** = seasonal climate model without photoperiod (see Methods). Lag in months. Dashes (—) indicate predictors not significant at any lag tested in the GAM, or wavelet R^2 not reported where the predictor is not physically meaningful at that phenophase scale. n/a = month (cyclic) and year (trend) smooths are internal GAM terms with no equivalent wavelet pair. Bold p-values: significance at $p < 0.05$. Full nested model comparison is given in Table S2.

Flowering						**Fruiting**				
Predictor	**Lag (Months)**	**edf**	**χ^2**	**p**	**Wav R^2**	**Lag (Months)**	**edf**	**χ^2**	**p**	**Wav R^2**
Insolation	1	1.00	5.43	**0.020**	0.551	—	—	—	0.191	0.492
Max. temperature	3	2.07	9.2	**0.016**	0.471	—	—	—	0.164	0.414
Min. temperature	3	1.00	4.63	**0.032**	0.423	6	3.01	18.9	**<0.001**	0.439
Rainfall	1	1.00	0.3	0.614	0.390	—	—	—	0.328	0.433
ENSO (ONI)	0	2.32	5.1	0.158	0.362	9	2.07	12.5	**0.004**	0.393
IOD (DMI)	6	2.47	11.0	**0.013**	0.355	11	4.09	15.8	**0.005**	0.374
Month (cyclic)	—	0.15	0.2	0.283	n/a	—	—	—	**<0.001**	n/a
Year (trend)	—	4.19	34.3	**<0.001**	n/a	—	—	—	**<0.001**	n/a

Wavelet R^2 colour legend (applies to Wav R^2 columns above):

Colour	Visual meaning	Mean R^2 range
	Extremely strong localised coherence	0.80 – 1.00
	Moderate to high coherence	0.50 – 0.79
	Weak, non-significant interaction	0.25 – 0.49
	Complete independence / no coherence	0.00 – 0.24

Figures

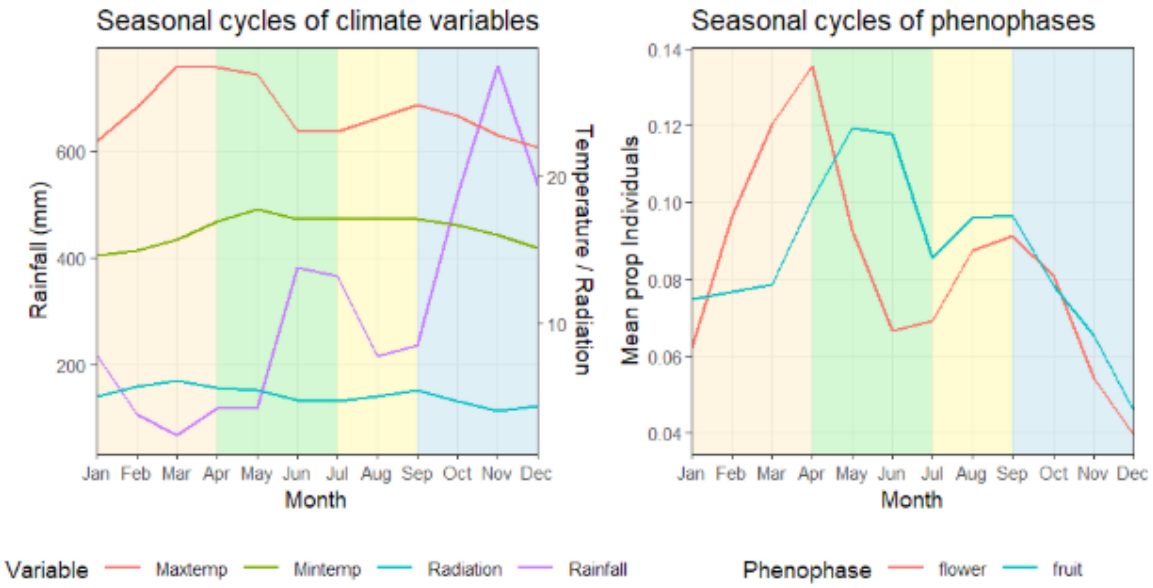


Figure 1

Summary of monthly mean maximum and minimum temperature, solar radiation and rainfall and flower and fruit phenophases in the wet evergreen forest at Kakachi in the Kalakad Mundanthurai Tiger Reserve (KMTR) of the Western Ghats where the long-term study was conducted between 1991-2012. Shaded regions (left to right) denote D1 (January–May), SWM (June–August), D2 (September) and NEM (October–December).

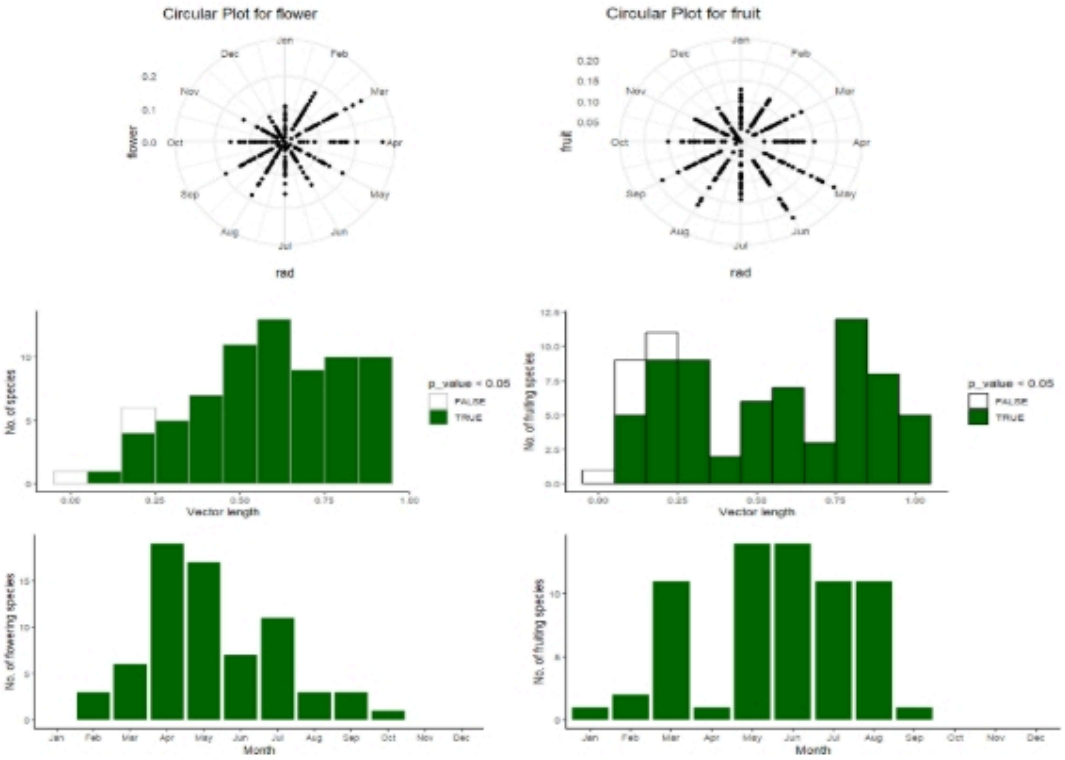


Figure 2

Phenological seasonality of flowering (left panels) and fruiting (right panels). Upper panels: circular (polar) plots of mean vectors, where vector angle represents mean date and vector length represents temporal concentration (0 = uniform, 1 = single date). Middle panels: histograms of number of species by temporal concentration. Lower panels: histograms of number of species by mean date.

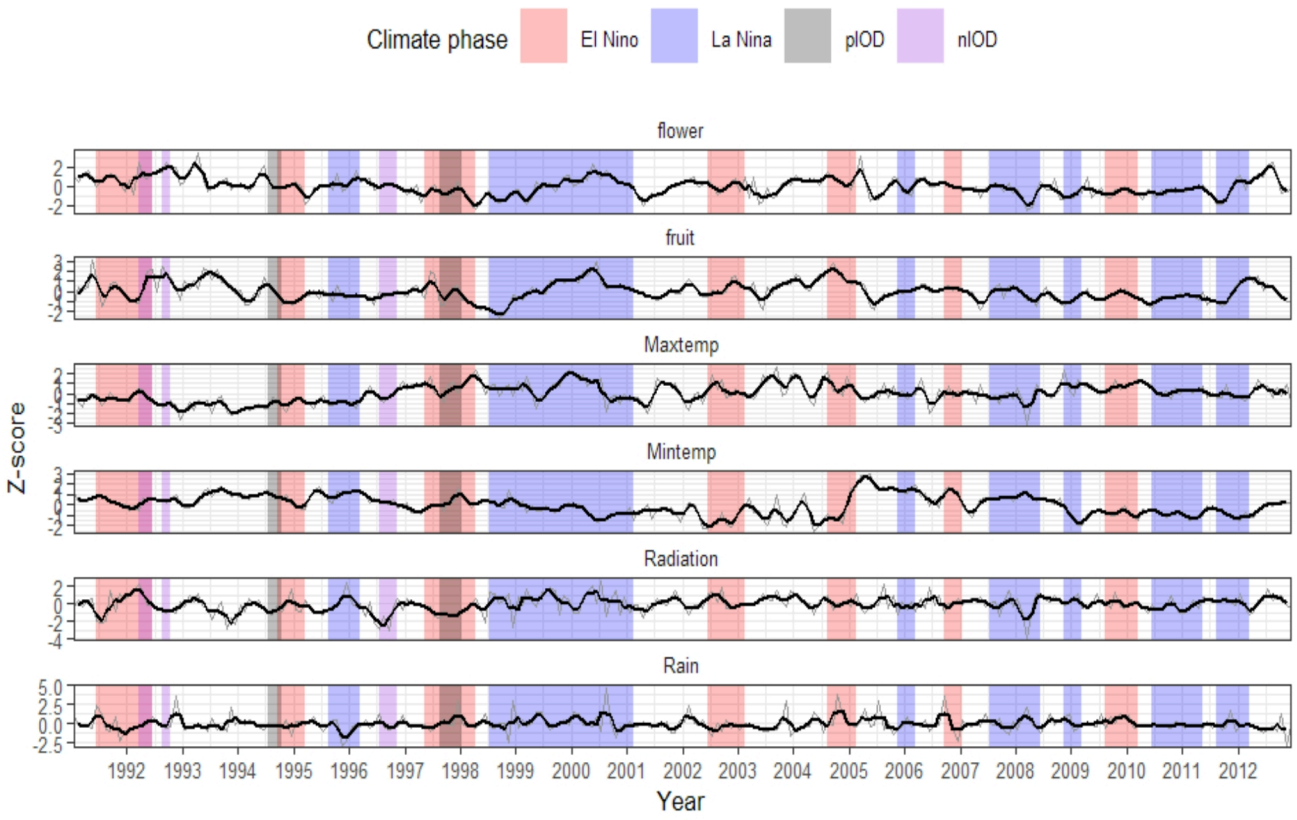


Figure 3

Temporal variation of phenological and climate variables. Monthly values of flowering, fruiting, and climate variables measured in the evergreen forest of Kakachi between 1991 and 2012 in relation to El Niño events (red shading) and La Niña events (blue). All series are seasonally detrended and normalized to zero mean and unit variance to facilitate visual comparison. The dark lines show 3-month running means; the thin gray lines show the monthly time series. X-axis ticks indicate January 1st. El Niño and La Niña events are identified based on Oceanic Niño Index values >0.5 °C and less than -0.5 °C, respectively, for at least five consecutive months. pIOD and nIOD are identified based on DMI values >0.5 °C and < -0.5 °C, respectively, for at least three consecutive months. Note the major El Niño and pIOD event in 1997–1998

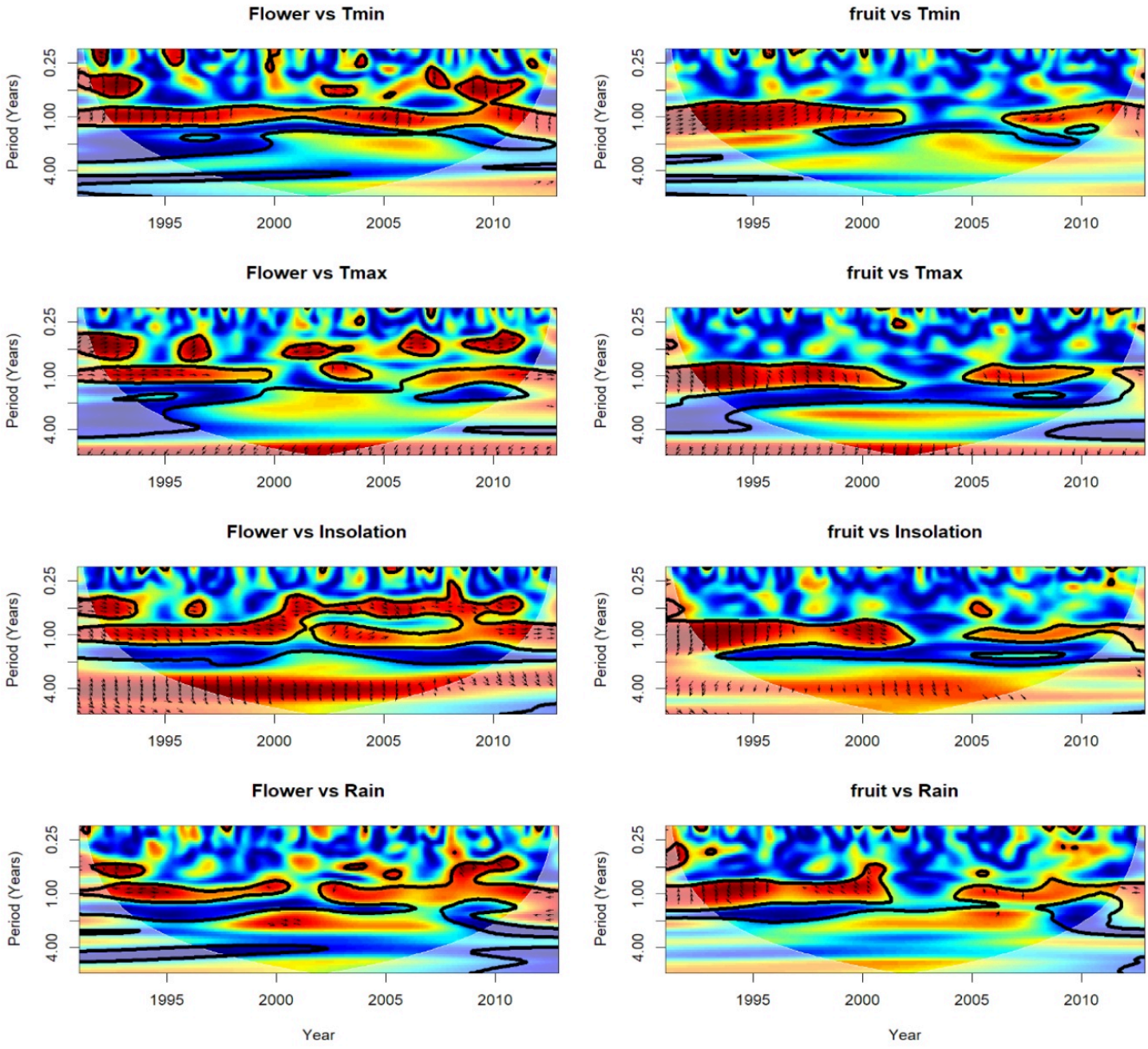


Figure 4

Wavelet coherence between flowering (upper panels) and fruiting (lower panels) and local climatic drivers (insolation, maximum temperature, minimum temperature, rainfall). Colour scale: warm colours indicate higher squared wavelet coherence; black contours enclose regions significant at $p < 0.05$ against red-noise surrogates; shaded cone of influence marks regions where edge effects may distort results. Arrows indicate phase relationships: → in-phase, ← anti-phase, ↑ phenophase leads climate, ↓ phenophase lags climate.

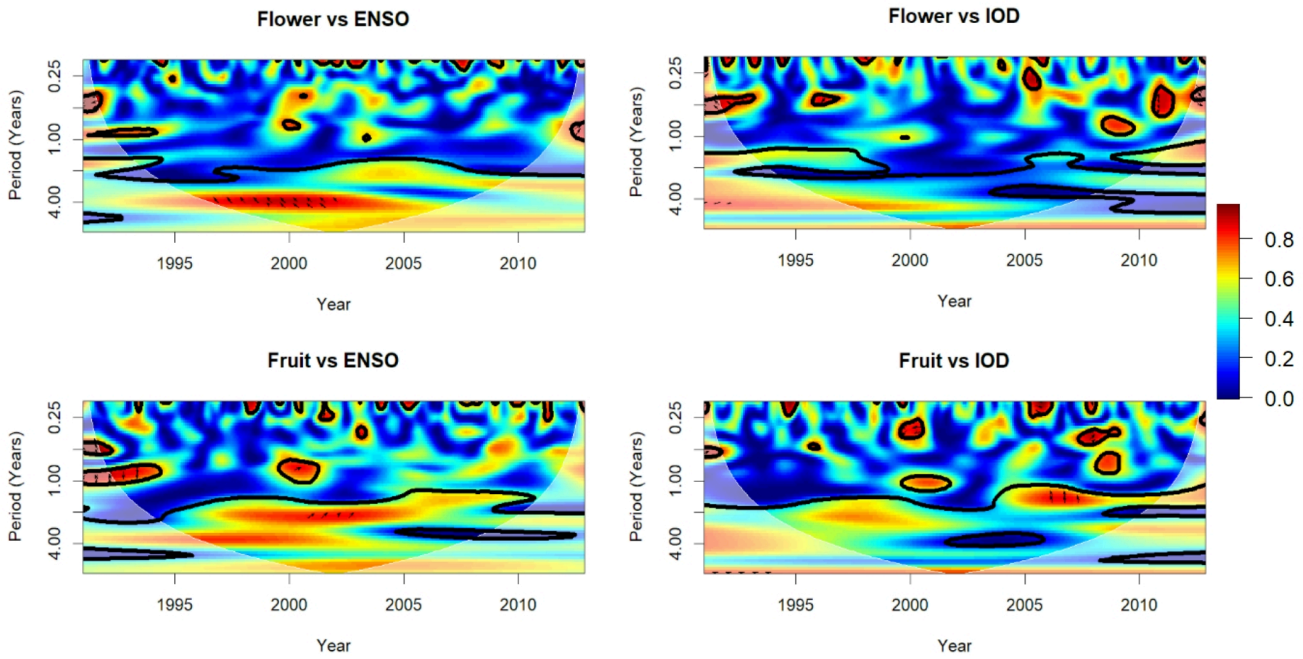


Figure 5

Wavelet coherence between ENSO (ONI, left panels) and IOD (DMI, right panels) and community-level flowering (upper panels) and fruiting (lower panels). Colour scale, contours and arrows as in Fig. 4. Flowering shows significant coherence with ENSO at annual-to-multi-annual periodicities during 1995–2005 and 2008–2012; fruiting shows significant coherence with both ENSO and IOD at 2–4-year periodicities, most pronounced around 1997–2001 and 2008–2012.

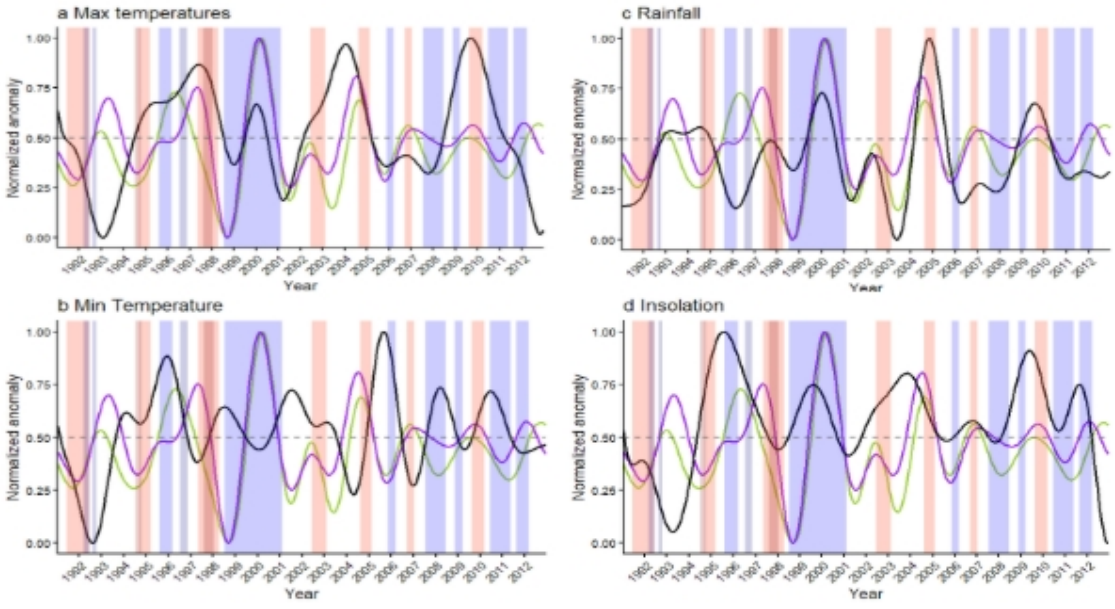


Figure 6

Band-pass-filtered interannual anomalies of flowering (green) and fruiting (purple) overlaid with ENSO and IOD events and individual climate variables (black lines), all normalised to 0–1 for comparison. Red shading: El Niño; blue: La Niña; dark red: positive IOD; light purple: negative IOD. The 1997–1998 compound El Niño–positive-IOD event is marked; note concurrent suppression of solar radiation and the subsequent fruiting rebound under La Niña–negative-IOD conditions.

Supplementary Files

This is a list of supplementary files associated with this preprint. Click to download.

- Suplimentary.docx